Korean J. Chem. Eng., **31**(11), 2020-2026 (2014)
DOI: 10.1007/s11814-014-0130-3

pISSN: 0256-1115
eISSN: 1975-7220

LaMer diagram approach to study the nucleation and growth of Cu_2O nanoparticles using supersaturation theory

Shahrzad Arshadi, Javad Moghaddam†, and Mohammadreza Eskandarian

Materials and Metallurgical Engineering Department, Advanced Materials Research Center, Sahand University of Technology, Tabriz, Iran
(*Received 11 March 2014 • accepted 29 April 2014*)

Abstract−Uptake to cuprous oxide (Cu_2O) nanoparticle synthesis with various particle sizes and shapes via supersaturation chemistry approach (LaMer model) has been conducted. Ascorbic acid and maltodextrine as reducing agents and polyvinylpyrrolidone (PVP) as a surfactant were utilized for synthesis of Cu_2O nanoparticles in aqueous solution. The narrow particle size range was achieved by controlling the kinetics of nucleation and growth of particles to satisfy LaMer theory. This mean was performed utilizing different reducing agents (ascorbic acid and maltodextrin) and also, changing the reducing agent addition condition. The results showed the reducing agent addition condition, varying the size of Cu_2O nanoparticles from 89 nm to 74 nm for drop-wisely and at-once routes, respectively. The samples were characterized by XRD, SEM, and UV-Vis spectroscopy. The results indicate the shape of as-prepared cuprous oxide nanoparticles have close relationship with thermodynamic and kinetic conditions, and also reducing addition condition.

Keywords: Cuprous Oxide, LaMer Diagram, Nucleation, Nanoparticles

INTRODUCTION

Nanoparticles are attracting increasing interest on account of their potential applications and unique features, which are strictly affected by their size, morphology, and three-dimensional structures [1-3]. In the vast majority of investigations, synthesis of high quality nanoparticles with a controlled size and shape has been a significant research focus in nanomaterials [4-6]. The foremost approach in the synthesis of nanoparticles is crystallization, So that controlling of the crystallization procedure has a significant role on the characteristics of products and allows manufacturers to prepare materials with desired and reproducible properties. The latest curiosity in nanocrystals and other related types of nanomaterials is a further illustration of the crystallization significance in science and technology [7]. At the nanometer range, the optical, electronic, and catalytic properties of nanomaterials are highly perceptive to their size and shape [8]. Consequently, the crystallization process (nucleation & growth) plays an important role in determining the crystal structure, shape, size and other morphological-related aspects of the nanomaterials. Therefore, a hypothetical approach to understand the mechanism of nanocrystals construction provides a greater control over the size, shape, and structure of nanocrystals and consequent ability to tune the above-mentioned properties simply by varying the crystallization conditions. One of the main aims of this approach of nanocluster science is the ability to prepare nanocrystals that have very narrow size distributions (which are called near-monodispersed). The major reason is to understand why nucleation and growth mechanism of nanocrystals in solution have been the subject of increasing study. However, concurrence between the theoretical models and experimental results is not so proper. This is a general shortcoming of nucleation theories. Accordingly, nucleation theories in general have little predictive power. It seems that a key goal of nucleation study is to improve the accuracy of theory [8]. Paying attention to the crystallization and growth approach from the viewpoint of application aspects seems to be an enormous feature of nanoparticle synthesis. One of these important areas is metal oxides and especially metal oxide nanoparticles. Dependency of characteristic of synthesized nanoparticles via crystallization-based routes is noticeable. Basically, metal oxides play an important role and are of paramount importance in many rapidly developing research areas such as the intersection of chemistry and materials science [9]. Potential applications include sensors, microelectronics, corrosion protection coatings, fuel cells, nanotechnology in general or catalysis [9,10]. Among the most widely used and characterized systems is copper, as well as its corresponding oxides [11-13]. Here, the complexity manifests itself by the presence of one important stable oxide with different properties for the copper system, which is, Cu_2O (T_m=1,235 °C, ρ= 6 gr/cm^3). As a representative p-type semiconductor with a band gap of about 2.2 eV, cuprous oxide (Cu_2O) nanomaterials have been widely used in solar energy conversion [14], gas sensors [15], photocatalysis [16,17], micro/nano electronics [18], lithium ion batteries [19] etc. To date, various well-dened Cu_2O nanostructures with different shapes and sizes, including hollow nano spheres [19,20], nano cages [21,22], nanowires [23,24], nano cubes [25,26], and octahedron [27,28] morphologies, have been synthesized. As is well known, the shape, size and microstructure are the main factors that determine the chemical and physical properties of nanomaterials. Therefore, it is still of great importance to prepare single-crystalline cubic nanoparticles and to control the particle size in a narrow size distribution over a wide adjustable range with simple one-step additive-free solution method at room temperature. At present, hydrothermal method [29], template method [30], and solution-phase syn-

†To whom correspondence should be addressed.
E-mail: moghaddam@sut.ac.ir, hastyir@yahoo.com

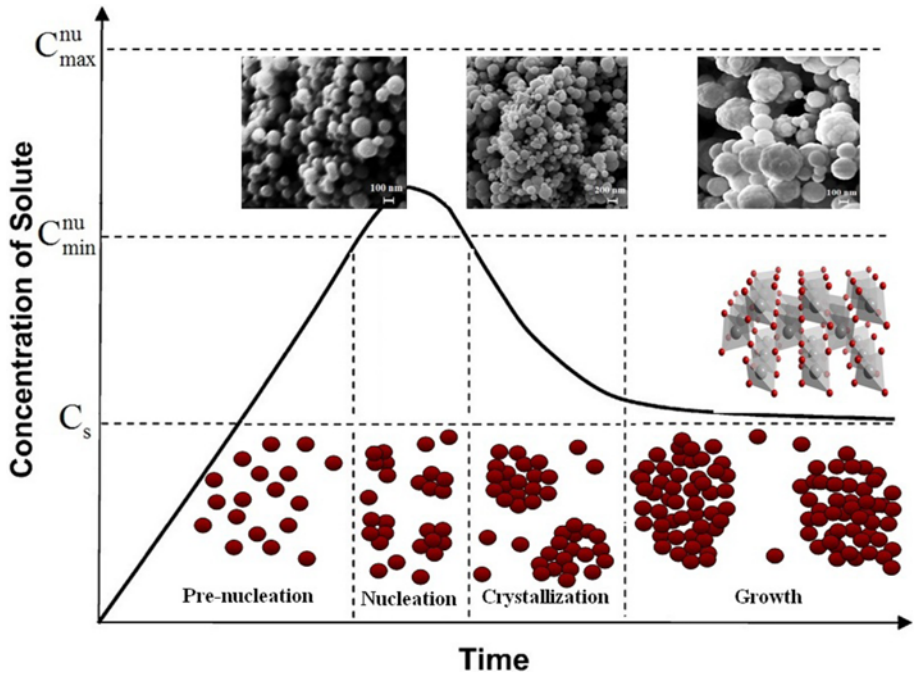

Fig. 1. LaMer diagram-Separation of nucleation and growth process.

thesis method [16,21,23-28,31] are the main wet-chemical methods developed for the synthesis of Cu_2O nanoparticles.

Since the employed synthesis method has significant aspect on the crystallization and phase transformation of acquired material, many challenges have been arisen to utilize a method which has sufficient prospective to prepare Cu_2O nanopowders with designed properties. Among the large number of theories proposed for the correlation between the nucleation and the growth of the generated nuclei, undoubtedly, the LaMer diagram suggested by LaMer and Dinegar [32] could clarify how monodispersed particles are obtained in a homogeneous solution. When the concentration of the precursor solute, C, goes up to the critical level for nucleation, C_{crit} (C_{min}), with its supply through generation in the system or feed from outside, the system virtually enters the nucleation stage. But it soon reaches the peak, C_{max}, because of the balance between the supply rate of the precursor solute and the consumption rate for the nucleation and the growth of generated nuclei. Then the curve declines owing to the increasing consumption of the solute for the growth of generated nuclei and reaches the critical level for nucleation again. This is the end of the nucleation stage. After that, the concentration of the solute still continues to be lowered by the growth of the generated stable nuclei under the supersaturation below the critical level for nucleation without renucleation. Such a clear separation between the nucleation and growth stages should yield monodispersed particles. Since the final number of the monodispersed particles is determined only in the nucleation stage and kept constant in the growth stage, and also, because controlling of particle size is equivalent to the control of particle number, the size control should be performed during the nucleation step in such a system [32]. LaMer theory competently describes the kinetic formation of particles which are controlled by diffusion of elements (particles, ions, etc). Sugimoto's model [33] describes the formation of nanoparticles that their nucleation and growth comport with the LaMer diagram and are controlled by diffusion. Fig. 1 shows the LaMer diagram as a schematic explanation for the formation procedure of monodispersed particles [32-34].

Present investigation involves a facile additive-free and room temperature solution process for the synthesis of uniform cubic (lattice) Cu_2O nanoparticles. At first, synthesis and operational parameters' effects on the nanoparticles and characteristics will be expressed and also, as a foremost approach, nucleation and the growth of Cu_2O nanoparticles will be discussed. Additionally, characteristics of nucleation and the growth mechanism of Cu_2O nanoparticles will be studied on the basis of LaMer theory. The effect of operational parameters on the characteristics of Cu_2O nanoparticles also has been considered.

EXPERIMENTAL PROCEDURE

1. Materials

Due to synthesis of the Cu_2O nanoparticles, copper acetate ($Cu(CH_3COO)_2 \cdot H_2O$), sodium hydroxide (NaOH), polyvinylpyrrolidone (PVP), ascorbic acid ($C_6H_8O_6$), and maltodextrin ($C_6H_{12}O_6$) were purchased from Sigma-Aldrich Co., Germany. All the chemicals were of analytical grade and used without further purification. Deionized water was used in the experiments.

2. Synthesis of Cu_2O Nanoparticles

Cu_2O nanoparticles were synthesized by using the following procedure. Typically, 0.05 g copper acetate, 0.2 g sodium hydroxide separately were dissolved into 100 ml, 20 ml of deionized water, and were mixed with constant stirring (0.0025 M and 0.25 M), respectively. As a resulting solution, aqueous $Cu(OH)_2$ was produced. In the next step, 0.39 g ascorbic acid as a reducing agent was dissolved in 15 ml deionized water (0.15 M) and subsequently was added to the $Cu(OH)_2$ solution prepared in the previous step. Within a few minutes, the deep blue solution gradually became colorless and then it turned burgundy type, which suggests the formation of Cu_2O col-

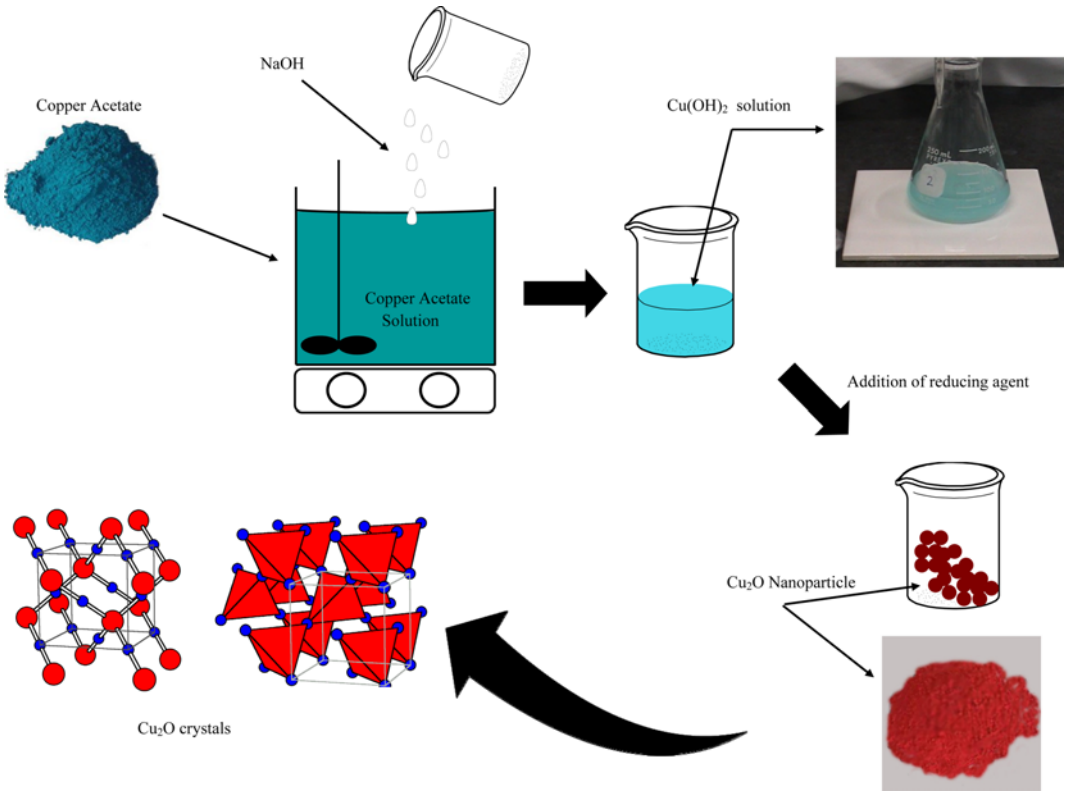

Fig. 2. Schematic representation of Cu_2O nanoparticles synthesis.

loid in presence of oxygen atmosphere. To continue, sediment was washed three times with distilled water and then the resulting colloidal was dried at 80 °C to obtain the powder form of Cu_2O sample, and it was used for further characterizations. A schematic representation for the preparation of Cu_2O nanoparticles is in Fig. 2. Additionally, Eq. (1) and Eq. (2) show the above mentioned procedure:

$$Cu(CH_3COO)_2 \cdot H_2O(aq)+2NaOH(aq) \rightarrow Cu(OH)_2(aq)+2NaCH_3COO(aq) \quad (1)$$

$$2Cu(OH)_2(aq)+C_6H_8O_6(aq) \rightarrow Cu_2O(s)+C_6H_6O_6(aq)+3H_2O \quad (2)$$

3. Effect of Reduction Rate

To study the effect of the reduction rate on the size and particle size distribution, after preparation of $Cu(OH)_2$ solution, that was obtained from a combination of sodium hydroxide and copper acetate, ascorbic acid as a reducing agent, was added in two different modes. Meanwhile, drop-wise and at-once procedure was used to evaluate the reduction rate for reducing agent.

4. Lamer Diagram for Ascorbic Acid as a Reducing Agent

To draw a LaMer diagram which is based on concentration changes at different times and due to create a more supersaturated and short-time nucleation, according to the results procedure mentioned in section 2.2, a stoichiometric amount of reducing agent was added at once to a solution containing $Cu(OH)_2$ three times and during 60 minutes (in the order of 0.5, 5, 10, 15, 20, 30 and 60 mins), samples of the solution in each time were analyzed by UV-Visible spectroscopy, then concentrations of Cu_2O nuclei were calculated. Finally, the last concentration which measured over an hour, was considered as equilibrium concentration.

5. Characterization

To probing the feature, especially crystallite size, X-ray diffraction using X'Pert Pro diffractometer (XRD-D8 ADVANCED-BRUCHERS AXS model, Germany), with a copper anode K_α radiation in a wavelength equal to λ=1.546 Å was utilized. To study the absorption spectrum of the samples, UV-Visible Spectrometer (Shimadzu UV-17000, Japan) was used. Scanning electron microscopy (SEM), images were obtained by TESCAN VEGAN II LMH (Czech Republic).

RESULTS AND DISCUSSION

1. Effect of Reduction Rate

XRD pattern of the reducing agent adding effect is illustrated in

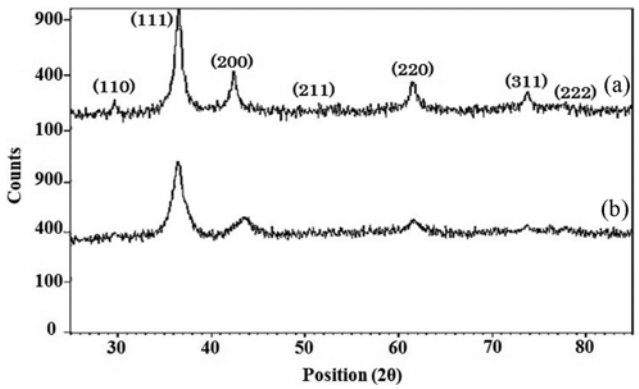

Fig. 3. Results of XRD analysis: Adding reducing agent (a) drop-wisely and (b) at-once.

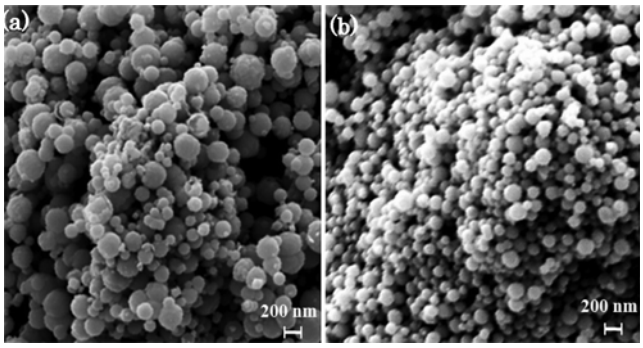

Fig. 4. SEM images of (a) slow and (b) fast reduction.

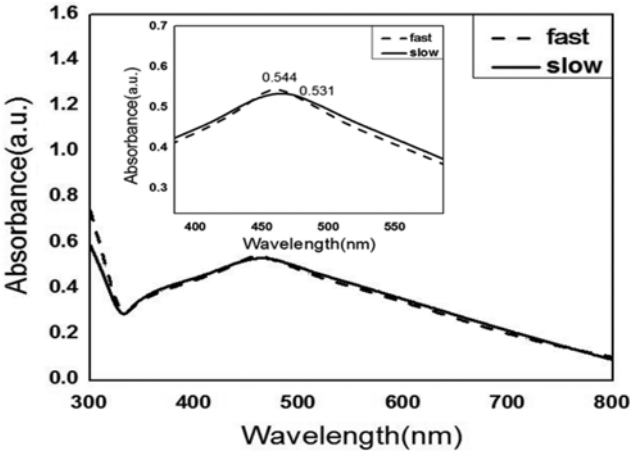

Fig. 5. UV-Vis peaks, related to the effect of solution reduction rate.

Fig. 3. As can be seen, review peaks indicate that at-once addition in comparison with drop-wised addition has the wider and lower intensity of the XRD peaks. These outcomes proposed the formation of smaller crystallites for at-once route. By considering of the integral width of (a) and (b) samples and placing in Scherer formula crystallite size of 89.13 and 74.01 nm were obtained for a and b method, respectively. Scanning electron micrographs of the two above-mentioned processes show that synthesized particles in at-once rout have the smaller diameter. SEM images of the dropwise and also at-once adding system are in Fig. 4. From SEM images of Fig. 4(a), it is known that by slow and staging reduction, the particle size distribution is wider and vice versa; when the solution is reduced quickly and at-once (Fig. 4(b)), the particle size distribution range will be smaller. In a recent case, since adding a reducing agent performed quickly, the reaction rate increases and the length of the nucleation period is cut short. So the vast majority of nuclei will be composed at a time and in a uniform range of particle sizes.

In addition, both above-mentioned solutions were checked due to absorption peaks using a UV-visible spectrophotometer. Results show that the peaks absorption edge of the at-once method is shifted to the lower wavelength, and since the particle size is proportional to the maximum wavelength (λ_{max}) [35-37], indicating the mean particle size is smaller, which is endorsing the results of XRD analysis and yet possessed of more sharp peaks, suggesting that the particle size distribution is smaller in this case. UV-Visible spectra and also larger magnification inset for two different solution reduction rate methods are presented in Fig. 5.

2. LaMer Diagram for Ascorbic Acid as a Reducing Agent

When ascorbic acid as reducing agent was used, even in less than stoichiometric amounts, the reaction was done very fast and cuprous oxide monomers were produced immediately. That is why at the first 30 seconds (0.5 min) of the reaction time, the first UV-Visible spectrum was considered. The results of analysis for samples prepared at different times appear in Fig. 6. According to the spectrum obtained in 0.5 min, a peak at wavelength of 452 nm is shown which is related to oxides of copper (I), and also a stronger peak is shown at a wavelength of 345 nm, which indicates the presence of bivalent copper complexes, related to some of the soluble $Cu(OH)_2$, which is still not reduced [38]. Over time, greater numbers of $Cu(OH)_2$ were converted to Cu_2O cores and with increasing concentrations of single valence core copper, the peak intensity of copper(I) oxide increased and the peak intensity of soluble $Cu(OH)_2$ weakened (declined); after 15 min of reaction, the peak of the soluble $Cu(OH)_2$ disappeared completely. By the way, increasing of absorption peaks is observed only in the first two sampling times (0.5 and 5 min), and after the peak time of 10 min, the absorption process tends to decrease. The latest spectrum after 60 min of reaction had a signifi-

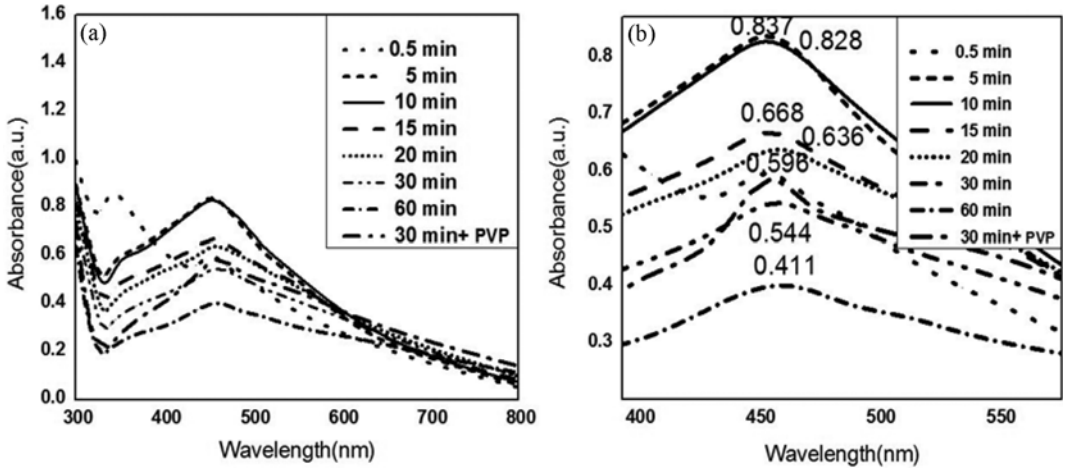

Fig. 6. Analysis of the UV/visible spectra at (a) 0.5, 5, 10, 15, 20, 30, 60 and 30+PVP and (b) In larger magnification.

cant decrease in peak intensity subsequently. Reduction in the absorption rate over time suggests the occurrence of phenomena such as Ostwald or agglomeration of particles [39], which consists of a large number of cuprous oxide nanoparticles, drawn together and for the spectrometer is considered as one particle; this leads to a significant reduction (decrease) in the concentration and amount of the absorption edge [40]. Also, with more time passing, the peak width is increased, which is caused by a broad particle size distribution, due to the number of particles formed by sticking together and has been resulting in the increasing of particle growth and particle size finally [41].

The two peaks of UV at 30 min are observed using polyvinylpyrrolidone (PVP) during the initial times of reaction (15 minutes); and the analysis taken at the time of 30 minutes compared to the case of absorption peak of the sample without PVP, the absorption rate will be higher, which indicates the presence of PVP, and can prevent the next agglomeration of particles. To determine the concentration of Cu^{+} ions at each sampling step, the absorption edge of each sample (Fig. 7), is put in the linear equation y=653.27X–0.0444, obtained from copper (I) oxide nanoparticles calibration curve. Changes in the concentration of Cu_2O cores versus time in Fig. 7 are plotted. Results verified that the chemical synthesis of copper (I) oxide nanoparticles follows the same plot in the LaMer diagram and similar to this graph. At the beginning of the process, an increase in concentration was observed, and after the nucleation period and beginning

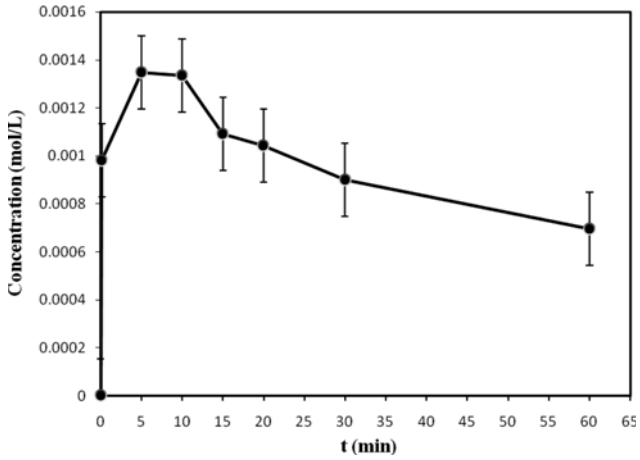

Fig. 7. Concentration of Cu+ changes over time (LaMer curve)-Ascorbic acid as reducing agent.

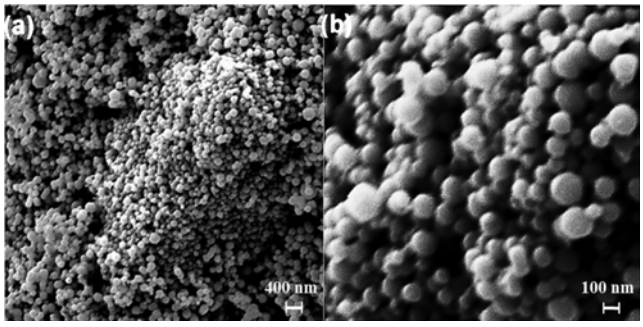

Fig. 8. SEM images of particles prepared after 30 minutes by ascorbic acid.

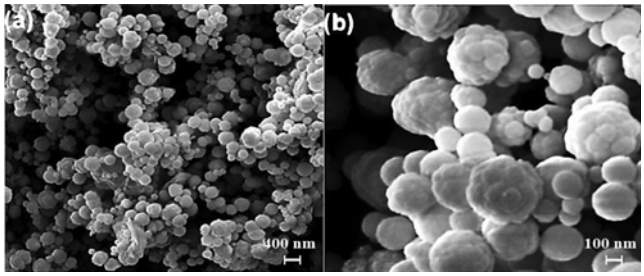

Fig. 9. SEM images of particles prepared after 60 minutes by ascorbic acid.

growth process, the concentration will be decreasing.

In Fig. 8, SEM images of the samples after 30min are illustrated, which show that after 30 min of reaction, the solution turned to powder and was analyzed by SEM. The results indicate that in the first 30 minutes of the reaction, there is no agglomeration between particles, but in Fig. 9, which corresponds to the powder obtained after 60 minutes of reaction, agglomeration between particles is clearly observed.

3. Change of the Reduction Factor and its Effect on the LaMer Diagram

To draw a LaMer diagram by using maltodextrin as reducing agent, a solution of copper acetate, sodium hydroxide, and maltodextrin ratio of $[Cu(CH_3COO)_2 \cdot H_2O] : [NaOH] : [C_6H_{12}O_6] \equiv 1 : 1 : 3$, in water bath (80 °C) was prepared by mechanical stirrer at 500 rpm. It was observed by changing the reducing agent from ascorbic acid to maltodextrin, the reaction proceeds slowly, which reflects the poor performance of maltodextrin in the reduction than ascorbic acid, so it requires more time to be reduced and for nucleation occur. As to the first three minutes of the reaction, there is a blue-green solution, indicating the lack of the formation of copper(I) oxide monomers; because of this after 4 min of reaction, when the solution was red, the first UV-Visible spectrum of the solution was taken. At different times (10, 15, 20, 30 and 60 min), solution samples were taken and analyzed by UV-visible analysis, respectively. The results of analyses of the samples prepared at the time of 4, 10, 15, 20, 30 and 60 minutes appear in Fig. 10. According to the spectrum obtained at 4 min, a weak peak of copper oxide (I) is observed at a wavelength of 458 nm, while the stronger peak at wavelength of 345 nm is seen to imply the not reduction of $Cu(OH)_2$ solution as the peaks of the reduction by ascorbic acid over time and the reduction of $Cu(OH)_2$ to Cu_2O nucleation; the peak intensity of the nucleus of cuprous oxide (I) increases and peaks of $Cu(OH)_2$ will be weaker, where over 20 min of reaction peak of $Cu(OH)_2$ is completely gone. Also, the rate of absorption peaks, indicating the intensity of the absorption peak increased until 20 minutes and after that has fallen. To investigate the concentration changes via LaMer approach Cu_2O nuclei concentration change versus time is plotted in Fig. 11. As can be seen, the chemical synthesis of nanoparticles of copper (I) oxide using maltodextrin as reducing agent follows the LaMer graph. Fig. 12 is related to the SEM images of the sample, which was analyzed after 60 min of the reaction, but 0.02 g amount of PVP was added to the solution after passing 15 min of the reaction. Results show that, while the maltodextrin is used as a reducing agent, due to slow response and long-term nucleation period, conditions will

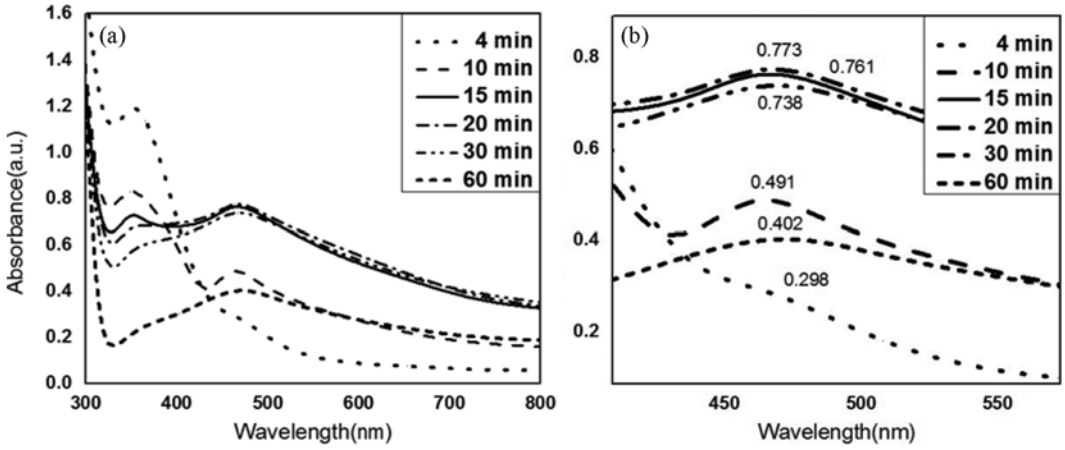

Fig. 10. Analysis of UV/visible spectra obtained at (a) 4, 10, 15, 20, 30 and 60 min and (b) In larger magnification.

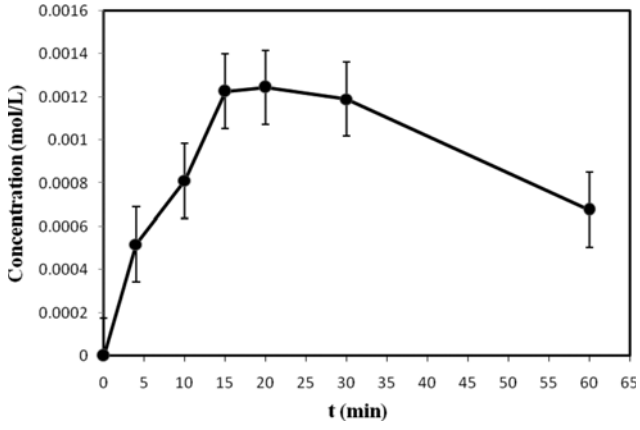

Fig. 11. Concentration changes over time (LaMer curve)-maltodextrin as reducing agent.

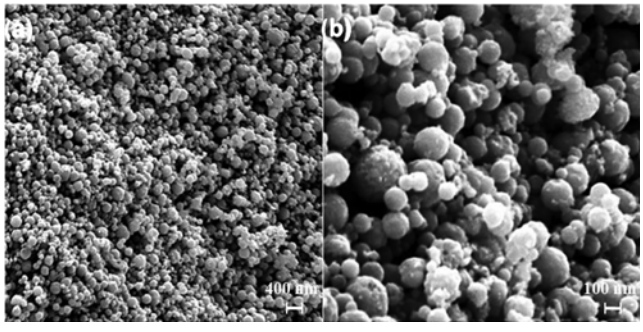

Fig. 12. SEM images of particles prepared after 60 minutes by maltodextrin.

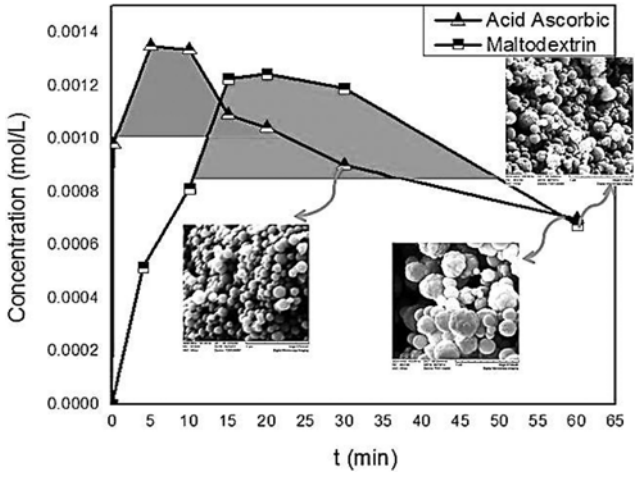

Fig. 13. Comparison of the two LaMer diagrams by reduction agents: Ascorbic acid and maltodextrin.

be similar to the mode in which the reduction factor was added dropwise to the original solution (slow reduction), and finally will lead to the formation of wide particle size distribution. The images also show that using PVP at the end of the nucleation period and before starting growth can prevent agglomeration of particles. Fig. 13 provides the results of related to using two different reducing agents (ascorbic acid and maltodextrin). Due to the slow response when using maltodextrin, the monomer concentration slope increases less and the time spent in the area of nucleation period and saturated will be increased. So the long period of nucleation caused particle growth and because of that, the particle size and distribution increased. In contrast, when using ascorbic acid, monomer concentration increased in a short time and the nucleation started immediately. This leads to supersaturation and the formation of cores in a short time, creating a thinner (sharp) nucleation area; and after all at the end of the nucleation period, growth and settling particle begins. Results show that the use of a strong reducer and increase in the reaction rate, the particles will be formed in smaller sizes and the same. This is due to the presence of abundant nucleation sites, which makes the nucleation mechanism overcome growth and the number of nuclei formed at a time will be much higher than when the reduction is weak.

CONCLUSION

Cu_2O nanoparticles using supersaturation approach successfully have been synthesized. LaMer model, as the most applicable theory in the scope of nucleation and growth of the particles, has been applied to consider the dependency of the crystallinity performance on the operational parameters. The results showed that some factors

accelerate the growth reaction, such as high temperature, creating more supersaturation and at-once addition of a strong reducing agent which cause short-time nucleation and separation of growth from nucleation. Consequently, particles with smaller size and size distribution will be formed. In addition, according to the UV-visible spectra obtained from the samples applying PVP as a stabilizer, in comparison with sample without PVP, the peak width is smaller, indicating a narrower size distribution and less agglomeration of particles. This work points out that Cu_2O nanoparticles with well-controlled shapes, sizes, and structures can be obtained by the optimization of thermodynamic and kinetic parameters.

ACKNOWLEDGEMENT

Authors gratefully thank the Zanjan Zinc Khalessazan Industries Company (ZZKICo), for their cooperation.

REFERENCES

1. M. A. El-Sayed, *Acc. Chem. Res.*, **37**, 326 (2004).
2. A. P. Alivisatos, *Endeavour*, **21**, 56 (1997).
3. A. P. Alivisatos, *Science*, **271**, 933 (1996).
4. Y. Yin and A. P. Alivisatos, *Nature*, **437**, 664 (2005).
5. C. B. Murray, S. Sun, H. Doyle and T. Betley, *Mater. Res. Bull.*, **26**, 985 (2001).
6. X. Peng, J. Wickham and A. P. Alivisatos, *J. Am. Chem. Soc.*, **120**, 5343 (1998).
7. S. Mahshid, M. Askari, M. Sasani Ghamsari, N. Afshar and S. Lahuti, *J. Alloys Compd.*, **478**, 586 (2009).
8. E. E. Finney and R. G. Finke, *J. Colloid Interface Sci.*, **317**, 351 (2008).
9. R. Rioux (Ed.), *Model systems in catalysis: single crystals to supported enzyme mimics*, Springer, New York (2010).
10. J. A. Rodriguez, *Synthesis, Properties and applications of oxide nanomaterials*, Wiley-VCH, Weinheim (2007).
11. B. Delmon, G. Ertl, H. Knözinger and J. Weitkamp (Eds.), *Handbook of heterogeneous catalysis*, Wiley-VCH, Weinheim (1997).
12. H. H. Kung, *Transition metal oxides: surface chemistry and catalysis*, Elsevier, Amsterdam (1989).
13. X.Wang, J. C. Hanson, A. I. Frenkel, J. Y. Kim and J. A. Rodriguez, *J. Phys. Chem. B*, **108**, 13667 (2004).
14. A. O. Musa, T. Akomolafe and M. J. Carter, *Sol. Energy Mater. Sol. Cells*, **51**, 305 (1998).
15. J. T. Zhang, J. F. Liu, Q. Peng, X. Wang and Y. Li, *Chem. Mater.*, **18**, 867 (2006).
16. Z. Zheng, B. Huang, Z. Wang, M. Guo, X. Qin and X. Zhang, *J. Phys. Chem.*, **113**, 14448 (2009).
17. W. C. Huang, L. M. Lyu, Y. C. Yang and M. H. Huang, *J. Am. Chem. Soc.*, **134**, 1261 (2012).
18. P. Poizot, S. Laruelle, S. Grugeon, L. Dupont and J. M. Taracon, *Nature*, **407**, 496 (2000).
19. Y. J. Lee, S. Kim, S. H. Park, H. Park and Y. D. Huh, *Mater. Lett.*, **65**, 818 (2011).
20. L. Zhang and H. Wang, *J. Phys. Chem.*, **115**, 18479 (2011).
21. C. Lu, L. Qi, J. Yang, X. Wang, D. Zhang and J. Xie, *Adv. Mater.*, **17**, 2562 (2005).
22. C. H. Kuo and M. H. Huang, *J. Am. Chem. Soc.*, **130**, 12815 (2008).
23. Z. C. Orel, A. Anžlovar, G. Dražić and M. Zigon, *Cryst. Growth Des.*, **7**, 453 (2007).
24. P. Grez, F. Herrera, G. Riveros, R. Henríquez, A. Ramírez and E. Muñoz, *Mater. Lett.*, **92**, 413 (2013).
25. H. Bao, W. Zhang, D. Shang, Q. Hua, Y. Ma and Z. Jiang, *J. Phys. Chem.*, **114**, 6676 (2010).
26. C. H. Kuo, C. H. Chen and M. H. Huang, *Adv. Funct. Mater.*, **17**, 3773 (2007).
27. Y. Xu, H. Wang, Y. Yu, L. Tian, W. Zhao and B. Zhang, *J. Phys. Chem.*, **115**, 15288 (2011).
28. Y. Zhang, B. Deng, T. Zhang, D. Gao and A. W. Xu, *J. Phys. Chem.*, **114**, 5073 (2010).
29. Z. Zhang, H. Che, Y. Wang, J. Gao, L. Zhao and X. She, *Ind. Eng. Chem. Res.*, **51**, 1264 (2012).
30. E. Ko, J. Choi, K. Okamoto, Y. Tak and J. Lee, *ChemPhysChem*, **7**, 1505 (2006).
31. L. Gou and C. J. Murphy, *Nano Lett.*, **3**, 231 (2003).
32. V. K. LaMer and R. H. Dinegar, *J. Am. Chem. Soc.*, **72**, 4847 (1950).
33. T. Sugimoto, *J. Colloid Interface Sci.*, **309**, 106 (2007).
34. T. Sugimoto, F. Shiba, T. Sekiguchi and H. Itoh, *Colloids Surf., A*, **164**, 183 (2000).
35. A. G. V. Poot, G. R. Gattorno, O. E. S. Dominguez, R. T. P. Diaz, M. Pesqueira and G. Oskam, *Nanoscale*, **2**, 2710 (2010).
36. D. Ma, H. Liu, H. Yang, W. Fu, Y. Zhang, M. Yuan, P. Sun and X. Zhou, *Mater. Chem. Phys.*, **116**, 458 (2009).
37. R. Viswanatha and D. D. Sarma, *Chem. Eur. J.*, **12**, 180 (2006).
38. Y. Bai, T. Yang, Q. Gu, G. Cheng and R. Zheng, *Powder Technol.*, **227**, 35 (2012).
39. L. Wang, G. Wei, B. Qi, H. Zhou, Zh. Liu, Y. Song, X. Ang and H. Li, *Appl. Surf. Sci.*, **252**, 2711 (2006).
40. G. Gao, H. Wu, R. He and D. Cui, *Corros. Sci.*, **52**, 2804 (2010).
41. G. Carotenuto, S. Denicola and L. Nicolais, *J. Nanopart. Res.*, **3**, 469 (2001).